A modeling basis for predicting the initial sprinkler spray

Di Wu[a], Delphine Guillemin[b], André W. Marshall[a],*

[a]*Department of Fire Protection Engineering, University of Maryland, 3104 J.M. Patterson Building, College Park, MD 20742, USA*
[b]*Ecole Nationale Supérieure de Mécanique et d' Aerotéchnique (ENSMA), 86960 Futuroscope Chasseneuil Cedex, France*

Abstract

The performance of water-based fire suppression systems is governed by the dispersion of the water drops in the spray. Characterization of the spray is essential for predicting and evaluating the performance of these suppression systems. The dispersion of the spray is typically modeled using particle tracking methods. The accuracy of the spray characterization using this approach is quite sensitive to the initial spray specification. A physics-based atomization model has been developed for prediction of the initial spray. Inputs to this model include injector geometry, injection pressure, ambient environment, and suppressant fluid properties. This atomization model also accounts for the stochastic behavior of the physical processes governing spray formation and provides probability distributions of initial drop sizes and locations for the initial spray. This modeling approach can be integrated with drop dispersion models and CFD models to characterize spray dispersion in quiescent environments or evaluate suppression performance in fire environments. The drop size predictions using the proposed atomization model have demonstrated favorable agreement with actual sprinkler spray measurements over a range of operating conditions.
© 2007 Elsevier Ltd. All rights reserved.

Keywords: Sprinklers; Atomization; Suppression; Sprays

1. Introduction

Characterization of the water spray is critically important in evaluating the performance of water-based suppression systems. A recent comprehensive overview of water-based fire suppression is provided in Grant et al. [1]. The performance of these suppression systems is primarily evaluated through full-scale spray dispersion tests and actual fire suppression tests. It is difficult to extrapolate the spray dispersion test performance to real fire scenarios because of the potentially strong coupling between the fire and the spray. Alternatively, actual full-scale suppression tests are expensive making it difficult to generate sufficient test statistics for proper evaluation of the test results. Predictive models are needed to evaluate spray characteristics or to couple with fire models to predict suppression performance. In fact, the atomization model is a critical missing link in the modeling of suppressed fires. Sophisti-cated gas phase models are in place for predicting the fire dynamics like Large Eddy Simulation (LES). Furthermore, drop dispersion models are well defined for tracking the drops after the atomization process is complete [2]. However, a general model has yet to be provided for predicting the initial spray properties for sprinklers. The atomization model developed in this study is a first step in addressing this deficiency.

Some simple correlations have been developed for estimating characteristic drop sizes based on a few experiments [3–5]. These correlations can be used as primitive predictive models; however, they have a limited range of validity and are insensitive to many effects that are known to influence the initial spray behavior. The data in these correlations are obtained under quiescent 'cool' conditions. However, the elevated velocities and temperatures in real fires are expected to influence the atomization process. A robust physics-based approach capable of handling this coupling has been used to develop the atomization model in this study. The present work provides the modeling basis to support the design of new

*Corresponding author. Tel.: +1 301 405 8507; fax: +1 301 405 9383.
E-mail address: awmarsh@eng.umd.edu (A.W. Marshall).

suppression devices, characterization of spray details, or evaluation of the resulting suppression performance in the presence of a real fire.

Some experimental work has been conducted to characterize the details of the sprinkler spray. The results from these experimental investigations provide sprinkler design guidance and provide valuable information for the development of atomization and spray models. Dundas [4] provides drop size measurements for several sprinkler geometries along with a review of drop size data obtained in a variety of injectors. The data are correlated based on an expression first proposed by Heskestad [6], $d_{v50}/D_{orif} = C We^{-1/3}$, where d_{v50} is the volumetric median diameter, D_{orif} is the injection orifice diameter, and the Weber number, $We = \rho_l U^2 D_{orif}/\sigma$, is based on the liquid properties. The drop size data compiled by Dundas from various injectors demonstrates that the coefficient of proportionality, C, depends on the sprinkler geometry [4]. You's data reveal more insight into the dependency of the coefficient, C. His data clearly show that C increases with increasing injection orifice diameter for upright sprinklers [3]. Prahl and Wendt [7] measured flow patterns from an axisymmetric laboratory sprinkler and developed models to predict these flow patterns. Correlations along with assumed Rosin-Rammler distributions were used to estimate drop size. Initial drop locations were approximated based on wave instability concepts, and drop trajectories were determined from particle tracking. Adjustments were made to the modeling constants to match the predicted and measured flow patterns. More recently Widmann [8], Widmann et al. [9], Putorti et al. [10], and Sheppard [5] have characterized velocities and drop sizes from sprinklers using advanced diagnostics. Widmann used Phase Doppler Interferometry (PDI) to measure drop sizes and velocities from actual sprinklers having K-factors ranging from $7.2 \times 10^{-5}\,\mathrm{m^3\,s^{-1}\,kPa^{-1/2}}$ (3.0 gal min^{-1} psi$^{-1/2}$) to $1.35 \times 10^{-4}\,\mathrm{m^3\,s^{-1}\,kPa^{-1/2}}$ (5.6 gal min^{-1} psi$^{-1/2}$). This measurement technique provides detailed information at one point within the spray. Characterizing the overall spray with this technique is prohibitive because of the number of point measurements required to map out the spray distribution. Nevertheless, the drop size and velocity measurements were taken at a number of locations at a given plane to determine the mass flux distribution using the PDI technique. The mass flux obtained from these PDI measurements at specified locations compared favorably with mass flux measurements taken with collection tubes. Widmann also noted deviation from the $p^{-1/3}$ scaling law for drop size at low pressures (around 69 kPa), but obtained better agreement at higher pressures. Putorti measured drop size and velocity simultaneously using a two-color fluorescence technique in an axisymmetric sprinkler configuration. Putorti's measurements provide drop size/velocity correlations, drop size distributions, and drop trajectories. Sheppard measured velocities very close to the sprinkler ($\sim$0.2 m) to characterize the initial spray velocity using Particle Image Velocimetry (PIV). This technique allows for visualization of a cross-section of the spray. He presented these measurements in a spherical coordinate system having the origin located on the sprinkler centerline at a specified position between the orifice and the deflector plate. Sheppard showed the variation of radial velocity with polar angle (measured from the sprinkler centerline) at various azimuthal angles (measured from the sprinkler yoke arms). He compared his velocity measurements with PDI measurements noting discrepancies due to differences in experimental configuration and biasing issues related to the differing measurement approaches used in the respective diagnostic techniques.

Predicting spray characteristics has proven to be challenging because of the complexity and stochastic behavior of the breakup process. In fact, it is common to simply characterize the sprinkler spray using correlations, or curve fits, of available experimental data. These experimental data are often obtained at conditions well outside of the operating conditions of interest. However, Dombrowski and Johns [11] developed an actual atomization model based on wave dispersion theory to predict drop size. This atomization model was developed using fan type injectors. Dombrowski described the atomization process in terms of the growth of waves on an infinite unstable sheet. He simplified the wave dispersion equations and integrated them to quantify the sheet breakup characteristics and then related the sheet disintegration to initial drop characteristics. This wave dispersion model has been successfully used by Rizk for various types of fuel injection systems [12] and is applied to sprinklers in the current study. Marshall and di Marzo [13] have developed a complete atomization model for sprinklers by integrating a film formation sub-model proposed by Watson [14] with a sheet disintegration sub-model proposed by Dombrowski and Johns [11]. Furthermore, these models have been implemented with a modified stochastic formulation originally proposed by Rizk and Mongia [12]. The current study provides the details for this atomization modeling approach. Results from this atomization model are presented and comparisons are made with actual sprinkler measurements and correlations.

2. Model description

2.1. Atomization physics

A spray is formed by breaking up a volume of liquid into small drops. This process is referred to as atomization. Sprinklers use atomization to facilitate the dispersion of water over a large area to protect commodities not yet involved in the fire. The spray also delivers water to burning materials and decreases the burning rate by reducing heat feedback to the fuel surface. Moreover, atomization greatly increases the surface area of the injected volume of water. In the case of finely atomized water mist sprays, this increased surface area results in

enhanced evaporative cooling of the hot smoke from the fire and displaces air with inert water vapor. These effects result in abatement or even extinguishment of the fire.

For sprinkler sprays, the atomization consists of three distinct stages. These stages are clearly illustrated in Fig. 1. First, the jet formed at the exit of the injection orifice impinges on a deflector plate to form a thin film that flows along the plate. This film travels beyond the surface of the plate to form an unconfined expanding sheet. This sheet breaks up more readily than the relatively large-diameter jet formed at the orifice exit. Next, aerodynamic waves are established on the liquid sheet, resulting from the inevitable small disturbances within the flow. These aerodynamic waves are unstable and grow to a critical amplitude which causes the sheet to break into ring-like ligaments. These ligaments are also subject to disturbances and the formation of aerodynamic waves. Finally, the waves on these ligaments grow to a critical amplitude and break the ligaments into small fragments which contract to form spherical droplets.

2.2. Deterministic model

The atomization model in this study consists of three sub-models based on the previously discussed sheet formation, sheet breakup, and ligament breakup processes generated by a jet impinging on an axisymmetric disc. This canonical or 'ideal' configuration is characterized as a first-step toward establishing an atomization model for the initial sprinkler spray. The 'ideal' geometry, although missing notable tine, frame arm, and boss features reveals many important trends related to the effect of changes in ambient conditions, injection conditions, and even geometry. Detailed descriptions of the sub-models for the 'ideal' sprinkler are provided in the following sections along with a discussion of the suitability and limitations of these canonical sub-models for application to actual sprinklers.

2.2.1. Sheet formation

The purpose of the sheet formation model is to predict the sheet thickness and velocity known to be important factors governing the atomization process as will be demonstrated in the following section. This sheet thickness and velocity is affected by viscous interaction with the deflector. For the 'ideal' configuration, free surface impinging jet theory is used to characterize this viscous interaction to determine the liquid film thickness and velocity at the edge of the deflector.

A water jet that impinges on a horizontal plate has been studied by Watson [14] using boundary-layer theory. Watson describes the radial spread of a liquid jet over a horizontal plane by four distinct flow regions. Fig. 2 shows these four regions.

Region I: The stagnation region ($r_{\text{stag}} = O[r_{\text{o}}]$, where r_{o} is the radius of the jet). The speed outside the boundary layer
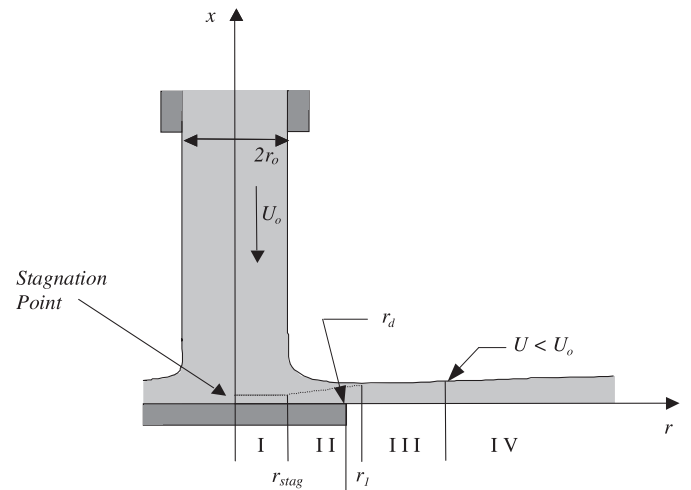

Fig. 2. Sprinkler jet forming a viscous film as it impinges against the deflector. The effect of the wall on the film can be treated analytically by considering the dynamics in four separate regions.
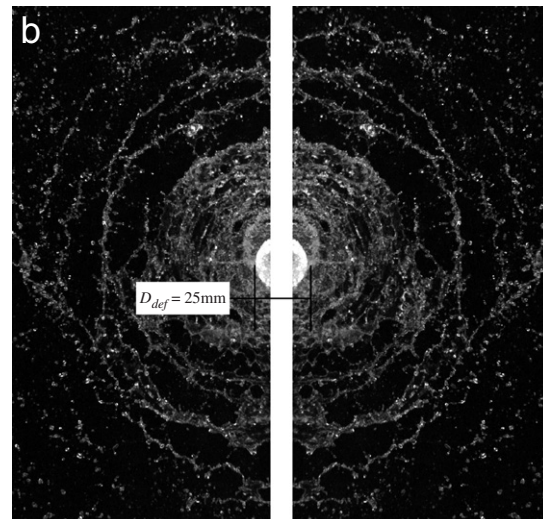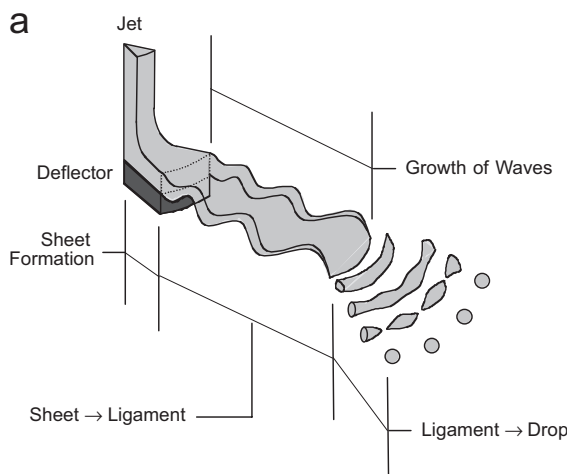

Fig. 1. (a) Illustration of the atomization process in conventional sprinklers [2]. (b) Photograph of the atomization process.

rises rapidly from zero at the stagnation point to U_o, the speed with which the jet strikes the deflector. The effect of the wall is contained in a very thin boundary layer, which is small compared to the film thickness.

Region II: The boundary layer region with Blasius similarity solution. The speed outside the boundary layer is unaffected by the layer and remains almost constant and equal to U_o. In this region, the boundary layer grows until the wall influences the entire thickness of the film.

Region III: The transition region. The whole flow is of boundary layer type with velocity profile given by the Blasius solution. The free surface is perturbed by the viscous stresses. The velocity profile changes as r increases; however, the velocity at the free surface remains nearly equal to U_o.

Region IV: In this region, the speed of the free surface decays more quickly with r. Velocity profiles in this region can be described by a non-Blasius similarity solution.

Watson's theory provides region specific expressions for the layer thickness based on the radial location for laminar and turbulent flows. The initial thickness of the sheet is given by the layer thickness at the edge of the deflector. The deflector diameter is thus an important parameter governing the atomization process. Typically, only Region I and Region II have to be considered in sprinkler flow configurations. However, the film has persisted beyond Region II in a few of the cases studied.

Assuming the motion in the layer is turbulent, for a deflector diameter corresponding to a radial location within Region II where $r_d < r_l$ (as shown in Fig. 2), the sheet thickness is given by

$$h_d = \frac{r_o}{2r_d} + C_1 \times \left(\frac{7v_l}{U_o}\right)^{1/5} r_d^{4/5}, \tag{1}$$

where r_l is the radial location where the boundary layer reaches the surface (boundary of Region II), r_o is the hydraulic radius of the jet, v_l is the liquid kinematic viscosity, r_d is the radius of the deflector plate, U_o is the initial speed of the jet, and $C_1 = 1.659 \times 10^{-2}$, which is a coefficient determined from the similarity analysis performed by Watson. It should be noted that this coefficient will change with sprinkler injection geometry. Other coefficients from the similarity analysis are included in subsequent equations and are denoted as C_i.

For deflector diameter corresponding to a radial location beyond Region II, the sheet thickness is given by

$$h_d = C_2 \times \left(\frac{v_l}{Q}\right)^{1/4} \frac{r_d^{9/4} + l^{9/4}}{r_d}, \tag{2}$$

where Q is the flow rate of the jet, $C_2 = 0.0211$, l is an arbitrary constant length, which has to be determined by the conditions where the boundary layer reaches the free surface $(r = r_l)$. The expression for l is obtained by matching the sheet velocity at $r = r_l$ and is given by

$$l = C_3 \times r_o \left(\frac{Q}{v_l \, r_o}\right)^{1/9}, \tag{3}$$

where $C_3 = 4.126$.

The turbulent flow assumption is not always valid over the full range of operating conditions. A stability criterion has been provided by Watson to determine whether the flow is laminar or turbulent. From similarity analysis, Watson derived a critical jet Reynolds number, $Re = Q/v_l r_o = 25{,}700$, above which the flow is turbulent. In the cases presented in the current study, the jet Reynolds number always exceeds this critical Re for injection pressures above 5 kPa. Therefore, for most cases the region-specific expressions for turbulent flow are appropriate for calculating the thickness and velocity of the liquid sheet at the exit of the deflector. The details of the laminar film formulation can be found in Watson [14].

For a sprinkler, U_o can be calculated based on Bernoulli's equation assuming inviscid flow, so that

$$U_o = \left(\frac{2\Delta p}{\rho_l}\right)^{1/2}, \tag{4}$$

where Δp is given by the difference between the total injection pressure and the environmental pressure and ρ_l is the density of the liquid. The hydraulic radius of the jet can be expressed in terms of the sprinkler properties by the dimensional equation

$$r_o = \left(\frac{K}{\pi}\right)^{1/2} \left(\frac{\rho_l}{2}\right)^{1/4}, \tag{5}$$

where K is the sprinkler K-factor describing the flow characteristics of the sprinkler. The K-factor is typically expressed in units $\text{gal min}^{-1}\,\text{psi}^{-1/2}$ or $\text{m}^3\,\text{s}^{-1}\,\text{kPa}^{-1/2}$.

The average speed of the sheet when it leaves the deflector plate can be calculated by mass conservation, so that

$$U = \frac{Q}{2\pi r_d h_d} = \frac{K \Delta p^{1/2}}{2\pi r_d h_d}. \tag{6}$$

The speed of the sheet is assumed to be constant and equal to U throughout the breakup process. The change in velocity due to gravitational acceleration has been neglected because the breakup time is typically less than 10 ms, providing little time for gravitational acceleration. After the film leaves the deflector plate, the thickness of the sheet decreases continuously as it expands radially. The thickness of the sheet is given by

$$h = \frac{r_d h_d}{r}, \tag{7}$$

where h is the thickness of the sheet along its radial extent given by the radial location, r.

Watson's free surface boundary layer model captures viscous interaction between the film and the deflector in the 'ideal' disc configuration quite well. As previously discussed, for typical sprinkler sizes and operating conditions,

viscous interaction between the film and the deflector is limited. The boundary layer typically does not progress beyond Region II before reaching the edge of the deflector resulting in film thicknesses and associated velocities typically within 20% of inviscid values.

For an actual sprinkler, the film formation may deviate from that predicted by Watson's model resulting from complex three-dimensional effects. The combined effect of the sprinkler boss and tines may direct flow through gaps in the deflector causing it to deviate from the radial trajectory assumed for the 'ideal' configuration and causing viscous interactions with the geometry not accounted for by Watson's axisymmetric model. No provisions have been made to account for the aforementioned geometric effects in actual sprinkler configurations. These effects will undoubtedly cause profound differences in the initial flow direction. However with regard to the initial drop size, it should be noted that Watson's axisymmetric model predicts a relatively small viscous sheet thickening effect (important for atomization). Without measurements it is difficult to verify if the viscous interaction with the deflector in actual sprinklers is also small; however, this result would be consistent with the short length scales associated with the deflector geometry. Comparisons between drop size predicted with 'ideal' sprinklers and actual sprinklers in Section 3.1 should shed some light on the importance of viscous effects in actual sprinkler geometries.

2.2.2. Sheet breakup

The central mechanism for atomization in sprinklers is the breakup of the liquid sheet formed by the injector into ligaments. This process is easily observed in Fig. 1, which shows the sheet breakup process in the 'ideal' sprinkler geometry. Although this configuration closely resembles that of a sprinkler, it should be noted that the 'ideal' configuration does not include tines which are present in actual sprinklers. Nevertheless, even in a tined configuration, a radially expanding sheet or radially expanding sheet fragments are expected. To describe the liquid sheet breakup process, a wave instability concept is used, which assumes that the disintegration of a liquid sheet or a jet occurs when the waves imposed by the surrounding atmosphere reach a critical amplitude. The sheet breaks forming ligaments and drops are produced as the ligaments disintegrate. Using this concept, Dombrowski and Johns [11] developed equations describing one-dimensional wave growth in an infinite viscous liquid sheet and successfully applied them to describe the disintegration of radially expanding sheets generated with fan nozzles. The central mechanism for atomization is treated in this simplified theory and following Dombrowski the theory is applied to more complex configurations of practical interest (i.e. the 'ideal' sprinkler configuration or even actual sprinklers). The suitability of neglecting multi-dimensional wave dispersion effects that may impact wave growth in more complex configurations will be determined from the quality of model comparisons with actual sprinkler data presented in Section 3.1.

In this model, sinusoidal waves are assumed to travel on the surface of the liquid sheet. A force balance is performed on the undulating sheet considering inertial, pressure, viscous, and surface tension forces. After considerable reformulation and simplification, the force balance can be expressed in terms of the growth rate of the waves present on the liquid sheet [11]:

$$\left(\frac{\partial f}{\partial t}\right)^2 + \frac{\mu_l}{\rho_l}n^2\left(\frac{\partial f}{\partial t}\right) - \frac{2(\rho_a nU^2 - \sigma n^2)}{\rho_l T} = 0, \tag{8}$$

where f is the dimensionless total growth of the wave, σ the surface tension, n the wavenumber of the disturbance imposed on the liquid stream ($n = 2\pi/\lambda$), λ the wavelength, ρ_a the air density, ρ_l the liquid density, T the thickness of the liquid sheet, and μ_l the liquid viscosity.

To simplify the analysis of the atomization process, inviscid fluid is first considered with $\mu_l = 0$, so that Eq. (8) becomes

$$\left(\frac{\partial f}{\partial t}\right)^2 - \frac{2(\rho_a nU^2 - \sigma n^2)}{\rho_l T} = 0. \tag{9}$$

For a specified n, the wave growth rate increases as the sheet velocity increases, which leads to a shorter sheet breakup time. Similarly, decreased air density or increased liquid surface tension results in longer sheet breakup time.

Because the wave with the maximum growth leads to the breakup of the sheet, the corresponding critical wavenumber is of interest. Taking the derivative of f with respect to n and equating to zero yields the critical wavenumber with the maximum growth in the inviscid formulation:

$$(n_{inv})_{crit} = \frac{\rho_a U^2}{2\sigma}. \tag{10}$$

Since the wavelength is inversely proportional to the wavenumber, the critical wavelength which leads to the breakup of the sheet increases as the liquid surface tension increases but decreases as the air density or sheet velocity increases.

After substituting Eq. (10) into Eq. (9), the sheet breakup time can be determined by integrating Eq. (9) with respect to time. Assuming that the sheet velocity U will remain constant until breakup, the breakup radius, r_{sh}, can be determined from calculating the time taken to reach a critical dimensionless amplitude, $f_{crit, sh}$. This dimensionless amplitude, f, describes the ratio of the growing disturbance amplitude to the amplitude of infinitesimal initial disturbances at the initiation of the sheet. The critical value, $f_{crit, sh} = 12$, can be determined experimentally and has been found not to depend on operating conditions for plain jets and fan nozzle sheets [11,15]. However, in the more complex impinging jet configuration, $f_{crit, sh}$ may depend on the details of the injector configuration and possibly even the injection pressure, because of possible sensitivities of initial disturbance amplitudes to these parameters. Nevertheless, for this initial study

following previous researchers, a constant value, $f_{\text{crit, sh}} = 12$, is applied in this model.

Although the inviscid flow assumption simplifies the problem significantly and provides some insight into the governing parameters, it is not realistic. For wave growth on liquid films with finite viscosity, Eq. (8) is solved for $\partial f/\partial t$ which is then integrated to determine the time to reach breakup ($f_{\text{crit, sh}} = 12$). Critical breakup times are determined over a range of wavenumbers. The breakup time, $t_{\text{crit, sh}}$, is minimized with respect to the wavenumber, $n_{\text{crit, sh}}$, corresponding to the most unstable wave leading to sheet breakup. The viscous sheet breakup model is expected to provide higher fidelity than the inviscid model; however, the effect of flow turbulence on the wave growth still needs to be considered in future refinements.

The sheet is assumed to break up into ring-like ligaments having an inner radius equal to the breakup radius, $r_{\text{bu, sh}} = r_{\text{d}} + Ut_{\text{bu, sh}}$, a radial width given by $\lambda_{\text{crit, sh}}/2$, and a thickness given by the sheet thickness at breakup, and $h_{\text{bu, sh}}$ determined from the liquid mass flow. The mass of the ligament, m_{lig}, is thus given by

$$m_{\text{lig}} = \pi \rho_{\text{l}} h_{\text{bu, sh}} [(r_{\text{bu, sh}} + \pi/n_{\text{crit, sh}})^2 - r_{\text{bu, sh}}^2]. \tag{11}$$

An equivalent diameter for the ligament can be determined from

$$m_{\text{lig}} = \pi^2 \rho_{\text{l}} \frac{d_{\text{lig}}^2}{2} \left(r_{\text{bu, sh}} + \frac{d_{\text{lig}}}{2} \right). \tag{12}$$

The goal of the sheet breakup analysis is to find the critical wavenumber with maximum growth which causes the sheet breakup. The ligament diameter can then be obtained from the mass of the sheet fragment after breakup. The ligament diameter is governed by the critical sheet breakup wavelength, sheet thickness at breakup, and the sheet breakup location. The ligament diameter is most sensitive to the change of the critical sheet breakup wavelength, and it increases as the critical sheet wavelength increases.

2.2.3. Ligament breakup

The ligaments formed from the sheet breakup are also unstable and subject to the growth of dilatational waves along the axis of the ligament. This wave growth ultimately leads to fragmentation of the ligament into drops. This breakup mode can be predicted from a stability analysis on a cylindrical column considering only surface tension and viscous forces.

Aerodynamic forces are neglected because this force is normal to the axis of the ligament and will not contribute to the growth of dilatational waves along its axis. These assumptions for the treatment of ligament breakup are currently applied to the 'ideal' sprinkler geometry; however, a similar analysis would be equally applicable for ligaments formed in the actual sprinklers. The stability analysis provides a simple relationship [15] for the critical

ligament wavelength for breakup, $\lambda_{\text{crit, lig}}$, given by

$$\lambda_{\text{crit, lig}} = \pi \sqrt{2} d_{\text{lig}}. \tag{13}$$

This fragment will contract into a drop. Conserving fragment mass, the characteristic droplet diameter, d_{drop}, is

$$d_{\text{drop}} = d_{\text{lig}} \left(\frac{3\lambda_{\text{crit, lig}}}{2} \right)^{1/3}. \tag{14}$$

The number of drops that are formed after ligament breakup can be expressed as

$$N = \frac{6M_{\text{lig}}}{\rho_{\text{l}} \pi d_{\text{drop}}^3}, \tag{15}$$

determined by conserving mass between the ligament and the drops. Weber [15] also provides an expression for the breakup time as

$$t_{\text{bu, lig}} = 24 \left(\frac{2\rho_{\text{l}}}{\sigma} \right)^{1/2} \left(\frac{d_{\text{lig}}}{2} \right)^{3/2}. \tag{16}$$

The distance that it takes for the ligaments to disintegrate into drops is easily calculated from the ligament velocity, U, and $t_{\text{bu, lig}}$. The initial drop location, which is the total distance the liquid travels until drops are formed, is given by

$$r_{\text{drop}} = r_{\text{d}} + U(t_{\text{bu, sh}} + t_{\text{bu, lig}}). \tag{17}$$

These atomization relationships provide characteristic initial spray conditions for a given sprinkler geometry and injection pressure, fire condition, and liquid suppressant. The initial spray velocity, U, initial spray drop size, d_{drop}, and initial spray location, r_{drop}, are completely defined by Eqs. (6), (14), and (17), respectively. These quantities are determined from the sprinkler geometry (K, r_{d}), injection pressure drop (Δp), surrounding flow gas phase fire conditions (ρ_{a}, μ_{a}), and liquid properties (σ, ρ_{l}, μ_{l}). It should be noted that for the current formulation the velocity of the gas in the vicinity of the sheet was assumed to be zero; however, the sprinkler entrainment velocity and the fire-induced velocity may significantly change the relative velocity of the sheet. The relative velocity may be more appropriate for use in Eq. (6) depending on the symmetry of the gas phase flow.

2.3. Stochastic model

In real sprays, a multitude of drops with different sizes are created. In order to model this behavior, a stochastic analysis is introduced [12]. In the stochastic atomization formulation, random behavior with a physical basis is added into the drop formation model to obtain the distributed drop characteristics. This physics-based technique provides an alternative to specifying a standard distribution about a calculated characteristic drop size. The liquid sheet critical breakup amplitude, the liquid sheet breakup wavelength, and the ligament breakup wavelength

are treated stochastically. The stochastic model ultimately provides distributions for initial drop size and location.

In the deterministic model, the critical dimensionless breakup amplitude is assumed to be a constant. However, this critical condition may vary with the largely unknown distribution of initial disturbance amplitudes. In the stochastic model, the dimensionless critical sheet breakup amplitude is treated as a discrete random variable $f[m]$ defined over an m-element space to account for the assumed distribution of initial disturbances. This amplitude ratio $f[m]$ satisfies a normal distribution specified by the mean critical sheet breakup amplitude, $\bar{f} = 12$ and the fluctuation intensity, I_f. This fluctuation intensity is a modeling parameter defined as

$$I_f = \frac{\sigma_f}{\bar{f}}, \tag{18}$$

where σ_f is the standard deviation of $f[m]$. The random variable $f[m]$ is used in the wave dispersion model resulting in m different critical sheet breakup wavelengths, sheet breakup times, and sheet breakup locations. These distributed parameters will influence the subsequent ligament formation and breakup analysis.

In the sheet breakup model, the sheet is assumed to breakup into ring-like structures having radial width of one-half wavelength. These ring-like structures rapidly contract into torroidal ligaments, which in turn break up into drops. The sheet, of course, does not always break up into one-half wavelength fragments. In the stochastic model, the radial width of the ligament fragments, $\Delta r_{lig}[m, n]$, is treated as a discrete random variable based on a chi-square distribution defined for each of the m sheet breakup realizations over an n-element space. The chi-square distribution prevents the occurrence of negative fragment widths at high fluctuation intensities. The specified sheet breakup fluctuation intensity is defined as

$$I_{lig} = \frac{\sigma_{lig}[m]}{\overline{\Delta r_{lig}}[m]}. \tag{19}$$

This intensity and the mean ligament fragment width $\left(\overline{\Delta r_{lig}}[m] = \overline{\lambda_{crit, lig}}[m]/2\right)$ calculated from the model are used to determine the standard deviation of sheet fragment widths, $\sigma_{lig}[m]$. These quantities are used to define the chi-square distribution and the resulting ligament fragment widths, $\Delta r_{lig}[m, n]$.

Similarly, the ligament fragment widths, $\Delta w_{drop}[m, n, p]$ are given by a chi-square distribution. The specified fluctuation intensity,

$$I_{drop} = \frac{\sigma_{drop}[m, n]}{\overline{\Delta w_{drop}}[m, n]}, \tag{20}$$

and the mean ligament fragment width, $\overline{\Delta w_{drop}}[m, n] = \overline{\lambda_{crit, lig}}[m, n]$, defines this distribution. In all $m \times n \times p$ drop sizes are obtained in the stochastic model together with the number of drops at each of the possible drop sizes. In the current study, m, n, and p are specified as

1000, 50, and 50, respectively in order to obtain sufficient statistics for a smooth drop size distribution.

Guidance for I_f, I_{lig}, I_{drop} values have yet to be established from measurements. These parameters are expected to be influenced by the injector geometry and the injection pressure. Currently, these values can only be estimated until data or models are available to provide guidance on values for these parameters. Careful measurements are currently being conducted from experiments over a range of configurations and operating conditions to support continued development of the atomization model. Predictions have been shown to agree with measurements using parameter ranges $0.05 < I_f < 0.25$, $0.1 < I_{lig} < 0.3$, and $0.1 < I_{drop} < 0.3$.

3. Modeling results

3.1. Deterministic analysis

The deterministic atomization model can be used to evaluate the sensitivity of the spray to changes in fluid properties or sprinkler geometry. Fig. 3 shows initial drop size and location predictions as a function of ambient temperature and injection pressure for a sprinkler having $K = 7.7 \times 10^{-5} \, \text{m}^3 \, \text{s}^{-1} \, \text{kPa}^{-1/2}$ (3.2 gal min^{-1} psi$^{-1/2}$) and $D_{def} = 25 \, \text{mm}$. Injection pressures up to $483 \, \text{kPa}$ ($70 \, \text{psi}$) are presented, but the model can be used at much higher pressures. If the sheet Re exceeds approximately 10^5, an additional shear instability breakup mode (not included in the model) producing very small drops may become important. However, this condition is not realized in sprinklers even with large orifices operating at extreme
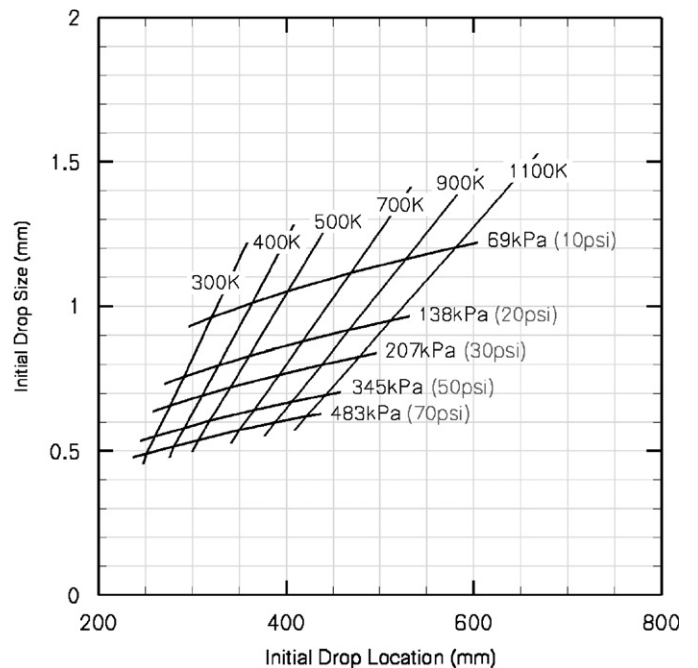

Fig. 3. Predicted initial drop conditions of a sprinkler spray as a function of injection pressure and ambient temperature, $D_{def} = 25 \, \text{mm}$ and $K = 3.2 \, \text{gal min}^{-1} \, \text{psi}^{-1/2}$.

injection pressures. These modeling results demonstrate the strong coupling between the ambient temperature and the atomization process. The model suggests that the initial spray at the time of sprinkler activation (sensor temperatures typically 330–370 K and gas temperatures much higher) and at various stages of the fire will differ from those measured under room temperature conditions. As the ambient temperature increases, the d_{drop} and $r_{bu,sh}$ increase. Increases in ambient temperatures result in lower ρ_a. These lower densities reduce the imbalance between critical aerodynamic pressure and surface tension forces, which is the driving force for wave amplification. The reduction in this driving force results in a slower wave growth rate and a corresponding longer $r_{bu,sh}$. Although these modeling results were obtained with the deterministic viscous model, the simpler inviscid wave growth equations can be used to better understand this behavior. In fact, combining Eqs. (9) and (10) reveals that the wave growth rate varies linearly with ρ_a. Furthermore, evaluation of Eqs. (11)–(14) reveals a double impact of ambient temperature on the drop size. Decreasing ρ_a results in both longer $r_{bu,sh}$ (and associated thinner $h_{bu,sh}$) and longer $\lambda_{crit,sh}$. These effects have opposing effects on d_{drop} resulting in relatively small increases in d_{drop} with increasing ambient temperature.

Fig. 3 also illustrates the effect of injection pressure, Δp, on the spray. Increases in Δp and associated increases in U will increase the imbalance between aerodynamic pressure and surface tension forces resulting in shorter breakup times. However, the increased U at higher Δp will have an opposing effect on $r_{bu,sh}$ resulting in only moderate reductions in $r_{bu,sh}$ with increases in Δp. This moderate reduction in $r_{bu,sh}$ (and associated thicker h) is overwhelmed by the substantial reduction in $\lambda_{crit,sh}$ with increased U as described in Eq. (10) resulting in significant reductions in drop size when Δp is increased.

The initial drop locations predicted in Fig. 3 are surprisingly long. Even at relatively high pressures, initial drops are not completely formed until 250 mm. These long drop formation distances are somewhat misleading. It should be noted that the atomization process initiates with sheet breakup, which occurs significantly upstream of the drop formation region as illustrated in Fig. 1(b). In fact, the sheet breakup times and ligament breakup times, which sum to the drop formation time are of the same order.

The deterministic atomization model can also be used to evaluate the impact of changing the sprinkler geometry. Fig. 4 shows the effects of changing the K-factor, which is a measure of the effective sprinkler orifice size, and the effects of changing the deflector size. The drop size and breakup length are significantly increased with increasing K-factor. These increases are due to the larger h, required by mass conservation. Increasing h increases the sheet stiffness resulting in a slower wave growth rate (less amplification) for a given driving force for wave growth (pressure/surface tension force imbalance). The slower wave growth rate results in longer $r_{bu,sh}$ resulting in
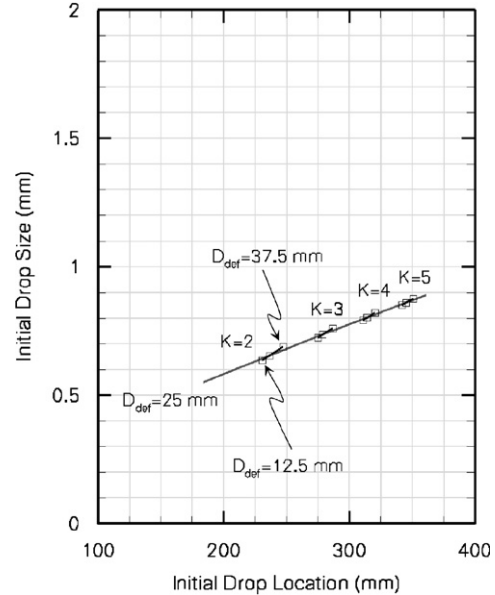

Fig. 4. Drop size and initial drop location predictions of a sprinkler spray at standard atmospheric conditions and $\Delta p = 138$ kPa (20 psi) while varying the diameter of the deflector and the sprinkler K-factor.

increased sheet thinning; however, the larger h resulting from the larger K-factor has a dominant effect on the drop size causing $\lambda_{crit,sh}$ and corresponding d_{drop} to increase. On the other hand, Fig. 4 shows that d_{drop} and $r_{bu,sh}$ are relatively insensitive to changes in the deflector size, r_d. Although increasing rd results in reduced U and increased h_d owing to increased viscous interaction between the film and the deflector, as discussed previously in Section 2.2.1 and as demonstrated in Fig. 4, the effect of this viscous interaction on d_{drop} is relatively small.

3.2. Stochastic analysis

The stochastic model provides a more realistic view of the spray where distributions of the initial drop sizes, locations, and velocities are predicted. These distributions are important when dispersion and vaporization calculations are required such as in suppression modeling. Figs. 5–7 show distributions for initial drop size, velocity, and location for a sprinkler having $\Delta p = 138$ kPa, (20 psi), $K = 3.2$ gal min^{-1} psi$^{-1/2}$ (7.7×10^{-5} m^3 s^{-1} kPa$^{-1/2}$), and $D_{def} = 25$ mm. Fluctuation intensities for the spray are also specified for the breakup process describing the chaotic behavior of the initial amplitude distribution ($I_f = 0.2$), the sheet fragmentation ($I_{sh} = 0.3$), and the ligament fragmentation ($I_{lig} = 0.3$). Fig. 5 shows that the drop size distribution at these conditions is well represented by a log-normal distribution. The median drop size is 0.92 mm with minimum drop size of 0.2 mm and maximum drop size of 2.8 mm compared with a characteristic drop size of 0.75 mm predicted by the deterministic model. Initial locations for ligaments and drops are provided in Fig. 6. It is apparent from this figure that drops do not

initiate from one point, but result from a spatially distributed process. The photograph included as Fig. 1(b) also demonstrates this behavior where drops and ligaments are observed in the same radial span. Fig. 6 shows that the sheet breaks up into ligaments between approximately 0.08 and 0.14 m. The sheet or ligaments may be present in this region. Ligaments begin to break up into drops at 0.18 m and continue to form drops until 0.40 m.

It is also useful to correlate the stochastic spray properties with drop size for specification of the initial

spray in CFD modeling. In this approach, a range of characteristic drop sizes is defined representing the entire spray. The initial location, velocity, and mass fraction are then specified for each characteristic drop size in this distribution. This method allows for the entire spray to be specified and tracked using a relatively small number of drops. Figs. 7–9 show the initial spray properties based on drop size. Fig. 7 shows that the smallest drop sizes are formed at the earliest times. Although the model specifies a uniform velocity distribution for the initial drops, the
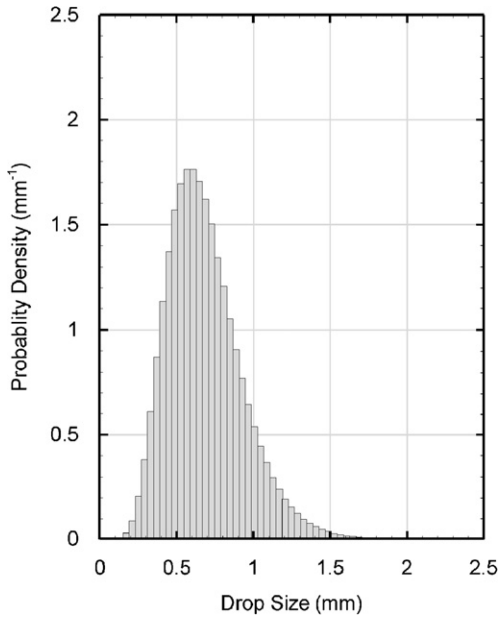
Fig. 5. Probability density function of initial drop size determined from stochastic model; $\Delta p = 138$ kPa (20 psi), $K = 3.2$ gal min^{-1} psi$^{-1/2}$, $D_{def} = 25$ mm, $I_f = 0.2$, $I_{sh} = 0.3$, $I_{lig} = 0.3$.

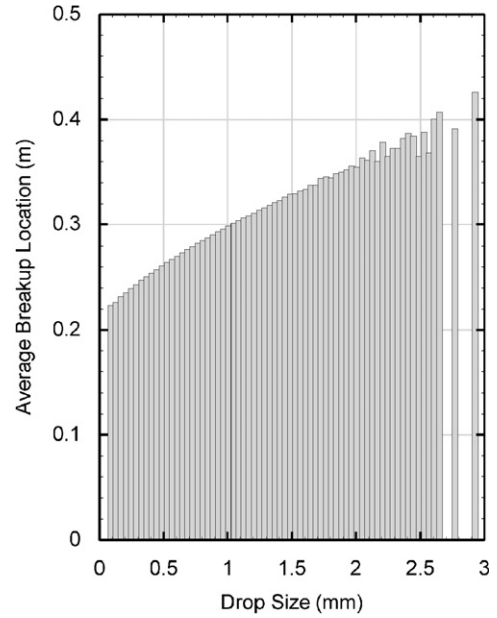
Fig. 7. Initial drop locations for characteristic drop sizes predicted with the stochastic model; $\Delta p = 138$ kPa (20 psi), $K = 3.2$ gal min^{-1} psi$^{-1/2}$, $D_{def} = 25$ mm, $I_f = 0.2$, $I_{sh} = 0.3$, $I_{lig} = 0.3$.
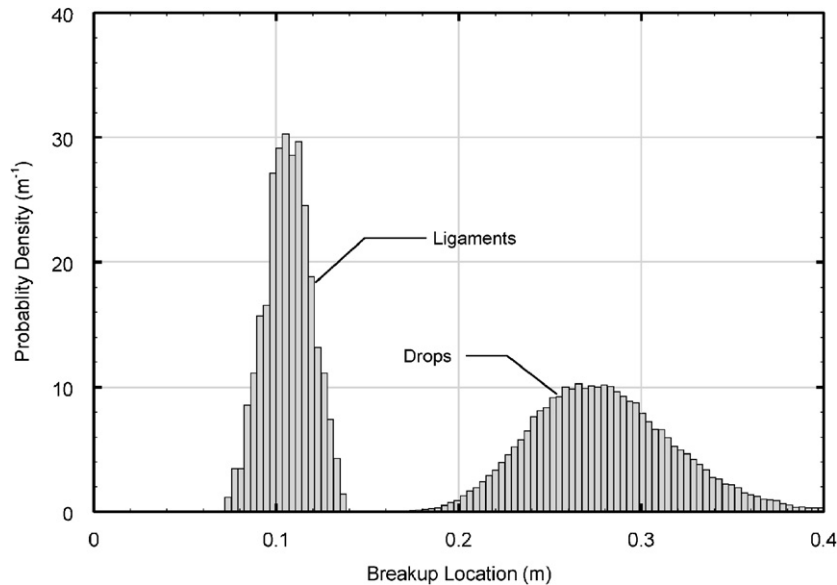

Fig. 6. Probability density function of initial drop breakup location determined from stochastic model; $\Delta p = 138$ kPa (20 psi), $K = 3.2$ gal min^{-1} psi$^{-1/2}$, $D_{def} = 25$ mm, $I_f = 0.2$, $I_{sh} = 0.3$, $I_{lig} = 0.3$.
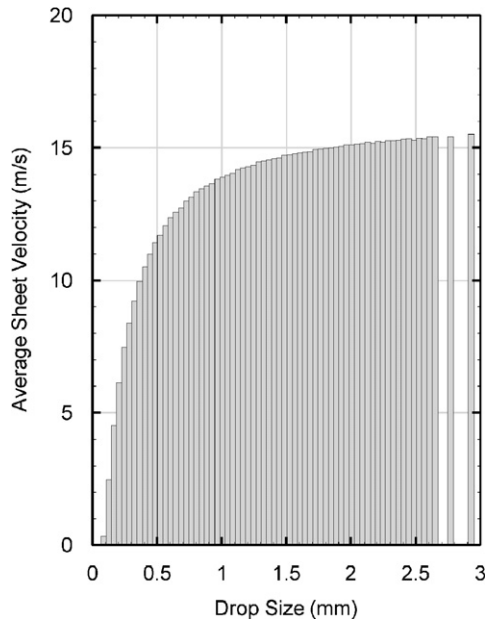
Fig. 8. Velocities for characteristic drop sizes predicted with the stochastic model and evaluated at a radial location of 0.65 m; $\Delta p = 138$ kPa (20 psi), $K = 3.2$ gal min^{-1} psi$^{-1/2}$, $D_{def} = 25$ mm, $I_f = 0.2$, $I_{sh} = 0.3$, $I_{lig} = 0.3$.
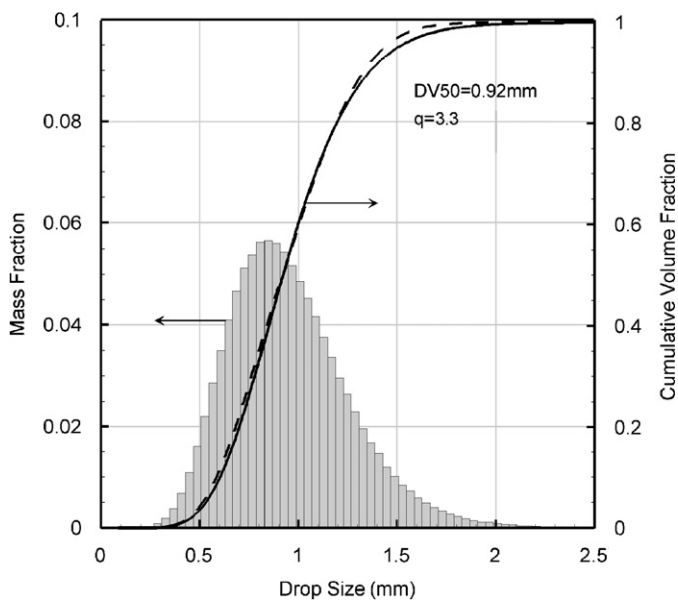

Fig. 9. Mass/volume fraction for characteristic drop sizes predicted with the stochastic model; $\Delta p = 138$ kPa (20 psi), $K = 3.2$ gal min^{-1} psi$^{-1/2}$, $D_{def} = 25$ mm, $I_f = 0.2$, $I_{sh} = 0.3$, $I_{lig} = 0.3$. —— Predicted cumulative volume fraction; - - - - Rosin-Rammler log-normal curve fit of prediction, $d_{v50} = 0.92$, $q = 3.3$.

positive location/size correlation results in a positive velocity/size correlation if the drops are tracked (allowing for drag forces) and viewed at a common downstream radial location. This positive velocity/size correlation evaluated at a radial location of 0.65 m and shown in Fig. 8 is consistent with measurements in sprinkler sprays [10]. Fig. 9 shows that the predicted drop size distribution is relatively narrow with very small drops (as well as the

very large drops) containing only a small fraction of the overall mass of the spray.

The drop size distribution is often provided in terms of the cumulative volume fraction. The cumulative volume fraction provides the percentage of the total spray volume contained in drop sizes smaller than a specified drop diameter. The predicted cumulative volume fraction is provided in Fig. 9. The Rosin-Rammler/log-normal distribution has been found to represent the cumulative volume fraction for sprinkler sprays. This distribution is given by

$$CVF = \begin{cases} (2\pi)^{-1/2} \int_0^{d_{CVF}} (q'd')^{-1} e^{-\frac{[\ln(d'/d_{v50})]^2}{2q'^2}} dd' & (d_{CVF} \leqslant d_{v50}), \\ 1 - e^{-0.693(d_{CVF}/d_{v50})^q} & (d_{v50} < d_{CVF}) \end{cases}$$

(21)

where CVF is the cumulative volume fraction of drops of diameter less than d_{CVF}, d_{v50} is the median volume diameter, q is a correlation coefficient, and $q' = 2((2\pi)^{1/2}(\ln2)q)^{-1} = 1.15/q$. The predicted cumulative volume fraction data are curve fit with the Rosin-Rammler/log-normal expression to determine if the predicted spray behaves like a typical spray and to determine the curve-fitting coefficients q for the distribution. The Rosin-Rammler/log-normal distribution having $d_{v50} = 0.92$ and $q = 3.3$ compares well with the predicted spray. This agreement shows that the atomization model is capable of predicting drop size distributions, which are at least qualitatively consistent with those expected from real sprinkler sprays. However, it should be noted that the value for q is higher than typical values for sprinklers ($q \sim 2.5$) indicating a narrow predicted distribution. Better agreement may be possible by adjusting the I parameters; however, tuning of the model is reserved until more detailed data is available.

3.3. Comparison with experiments

A more quantitative evaluation of the model was obtained by comparing model predictions with actual sprinkler data. As mentioned previously, no attempt has been made to adjust the model for the effect of tines; however, comparisons between the modeled 'ideal' configuration and actual sprinklers should shed some light on the ability of the model to capture the essential physics for sprinkler atomization.

Assuming negligible secondary atomization, it is reasonable to compare initial spray predictions with overall spray measurements. This is a reasonable assumption because secondary atomization does not occur for droplet $We \leqslant 12$ [16]. And according to our calculations droplet We exceeding 12 rarely occurs in sprinkler sprays even for large sprinklers operated at high pressures. Although nearfield data is not available, the invariance of Yu's measurements further downstream support this assumption [3]. Yu demonstrated that secondary atomization and
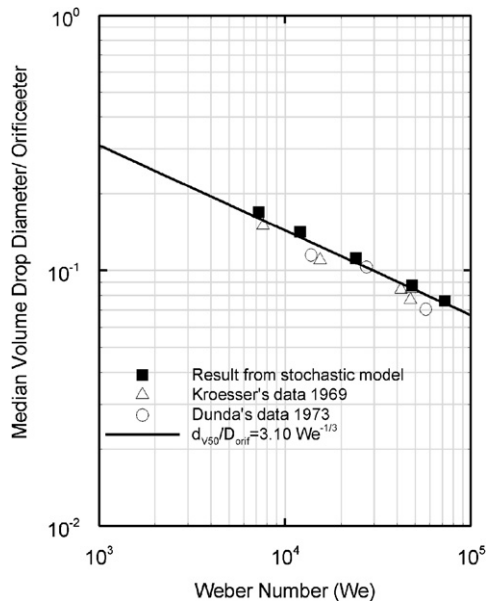
Fig. 10. Comparison between stochastic model predictions with sprinkler data using $I_f = 0.2$, $I_{sh} = 0.3$, $I_{lig} = 0.3$, $D_{orif} = 12.7$ mm, $D_{def} = 31$ mm, $\triangle$ Kroesser's data 1969, $\circ$ Dundas' data 1973, $\blacksquare$ stochastic model predictions, and —— $d_{v50}/D_{orif} = 3.10\, We^{-1/3}$.

coalescence is negligible in the farfield of his large sprinkler spray between 3 and 6 m. Fig. 10 shows the modeling predictions compared with data provided by Dundas [4]. Dundas showed that data from many sprinklers could be correlated by

$$\frac{d_{v50}}{D_{orif}} = C\, We^{-1/3}, \qquad (22)$$

where 50% of the spray volume is contained in drops smaller than d_{v50} (volume median diameter) and the *We* is based on the orifice diameter. In Dundas' research, the coefficient for 1/2 SSU Duraspeed, Reliable, and Grimes upright sprinklers was determined to be $C = 3.1$. Model drop size predictions for sprinklers with similar geometry ($D_{orif} = 12.7$ mm and $D_{def} \approx 31$ mm or $r_d \approx 15.5$ mm) were compared to the experimental data and the corresponding correlation at various injection pressures. These model predictions agree very well with the experimental data and the correlation curve. The good agreement between drop sizes predicted by the model and produced by several actual sprinklers over a range of injection pressures supports the validity of our modeling assumptions. Although, it should be noted that the model prediction used stochastic modeling parameters of $I_f = 0.2$, $I_{sh} = 0.3$, $I_{lig} = 0.3$ for all *We*. These fluctuation intensities were set somewhat arbitrarily; even so, they appear to have rational values. These modeling parameters primarily affect the drop size distribution, but also to a lesser extent modify the characteristic drop size. Better guidance for these values will be obtained as more detailed data in the breakup region of the spray is obtained. More actual sprinkler measurements should also reveal to what extent unmodeled

geometric details are contained within these parameters. The authors are currently conducting spray measurements in this region to build models for determining these fluctuation intensities.

4. Conclusions

An atomization modeling basis for sprinklers has been developed using free surface boundary layer and wave dispersion theories. The sprinkler is modeled as an axisymmetric impinging jet. The effect of the frame arms and tines are not currently incorporated into the model, but will be included in future refinements. The atomization model provides initial drop conditions that can be used to track an array of characteristic initial drop sizes that represent the entire spray. The atomization model predicts an initial spray having a realistic drop size distribution, which closely matches the Rosin-Rammler/log-normal expression. Despite the simplified configuration used to develop the model, median volume diameters, d_{v50}, calculated from predicted distributions show excellent agreement with actual drop size measurements from sprinklers.

References

[1] Grant G, Brenton J, Drysdale D. Fire suppression by water sprays. Prog Energy Combust Sci 2000;26:79–130.
[2] Borman GL, Johnson JH. Unsteady vaporization histories and trajectories of fuel drops injected in swirling air. SAE Paper 598C, 1962.
[3] Yu HZ. Investigation of spray patterns of selected sprinklers with the FMRC drop size measuring system. First international symposium on fire safety science, 1986, New York. p. 1165–76.
[4] Dundas PH. Technical report optimization of sprinkler fire protection the scaling of sprinkler discharge: prediction of drop size. FMRC serial no. 18792 RC73-T-40. Norwood, MA: Factory Mutual Research Corporation; June 1974.
[5] Sheppard DT. Spray characteristic of fire sprinklers. NIST GCR 02-838. Gaithersburg, MD: National Institute of Standards and Technology; 2002.
[6] Heskestad G. Proposal for studying interaction of water sprays with plume in sprinkler optimization program. Memorandum to C. Yao, June 16, 1972.
[7] Prahl JM, Wendt B. Discharge distribution performance for an axisymmetric model of a fire sprinkler head. Fire Saf J 1988;14: 101–11.
[8] Widmann JF. Phase droppler interferometry measurements in water sprays produced by residential fire sprinklers. Fire Saf J 2001;36: 545–67.

[9] Widmann JF, Sheppard DT, Lueptow RM. Non-intrusive measurements in fire sprinkler sprays. Fire Technol 2001;37:297–315.

[10] Putorti AD, Everest D, Atreya A. Simultaneous measurements of drop size and velocity in large-scale sprinkler flows using particle tracking and laser-induced fluorescence. Gaithersburg, MD: National Institute of Standards and Technology; 2003.

[11] Dombrowski N, Johns WR. The aerodynamics instability and disintegration of viscous liquid sheets. Chem Eng Sci 1963;18:203–14.

[12] Rizk NK, Mongia HC. Model for airblast atomization. J Propulsion 1991;7:305–11.

[13] Marshall AW, di Marzo M. Modeling aspects of sprinkler spray dynamics in fires. Process Saf Environ Prot Trans Inst Chem Eng Part B 2004;82:97–104.

[14] Watson EJ. The radial spread of a liquid jet over a horizontal plane. J Fluid Mech 1964;20:481–99.

[15] Weber Z. Zum zerfall eines flussigkeitstrahles (on the disruption of liquid jets). Angew Math Mech 1931;11:136–54.

[16] Pilch M, Erdman CA. Use of breakup data and velocity history data to predict the maimum size of stable fragments for acceleration-induce breakup of a liquid drop. Int J Multiphas Flow 1987;13:741–57.